THE PROTEIN SOCIETY

Molecular mechanism of bacterial Hsp90 pH-dependent ATPase activity

Yi Jin, Reyal S. Hoxie, and Timothy O. Street*

Department of Biochemistry, Brandeis University, Waltham, Massachusetts, 02453

Received 1 February 2017; Accepted 31 March 2017
DOI: 10.1002/pro.3174
Published online 6 April 2017 proteinscience.org

Abstract: Hsp90 is a dimeric molecular chaperone that undergoes an essential and highly regulated open-to-closed-to-open conformational cycle upon ATP binding and hydrolysis. Although it has been established that a large energy barrier to closure is responsible for Hsp90's low ATP hydrolysis rate, the specific molecular contacts that create this energy barrier are not known. Here we discover that bacterial Hsp90 (HtpG) has a pH-dependent ATPase activity that is unique among other Hsp90 homologs. The underlying mechanism is a conformation-specific electrostatic interaction between a single histidine, H255, and bound ATP. H255 stabilizes ATP only while HtpG adopts a catalytically inactive open configuration, resulting in a striking anti-correlation between nucleotide binding affinity and chaperone activity over a wide range of pH. Linkage analysis reveals that the H255-ATP salt bridge contributes 1.5 kcal/mol to the energy barrier of closure. This energetic contribution is structurally asymmetric, whereby only one H255-ATP salt-bridge per dimer of HtpG controls ATPase activation. We find that a similar electrostatic mechanism regulates the ATPase of the endoplasmic reticulum Hsp90, and that pH-dependent activity can be engineered into eukaryotic cytosolic Hsp90. These results reveal site-specific energetic information about an evolutionarily conserved conformational landscape that controls Hsp90 ATPase activity.

Keywords: chaperone; Hsp90; pH; ATP

Introduction

The highly conserved family of Hsp90 molecular chaperones (Hsp90α/β in the cytosol, Trap1 in mitochondria, Grp94 in the endoplasmic reticulum) are believed to interact with substrate proteins in their late folding stage.[1,2] Hsp90 has specific regulatory effects in eukaryotes because some Hsp90 substrate proteins are involved in cellular signaling and cell proliferation.[3–5] Therefore, Hsp90 has been a long-standing pharmaceutical target to inhibit the growth of cancer cells. The ability of Hsp90 to bind and hydrolyze ATP is critical for its function.[6,7] Indeed, the main class of Hsp90 inhibitors all prevent ATP binding.[8]

Hsp90 is a dimer in which each monomer has three domains: N-terminal (NTD, salmon, Fig. 1), middle (MD, sky blue) and C-terminal (CTD, lime).[9] The CTD contains a dimerization interface, and the NTD has a nucleotide binding site. The open state of Hsp90 is hydrolytically inactive. ATP binding stabilizes the closed, hydrolytically active, state of Hsp90.[10] Two closed states of Hsp90, symmetric[11] and asymmetric,[12] have been observed crystallographically. Although the role of structural asymmetry in Hsp90's ATPase cycle is not well established, functional asymmetry has been proposed for Hsp90/co-chaperone complexes[13–15] and Hsp90/substrate interactions.[16] Among the many conformational changes accompanying the open/closed transition, there is a large displacement of the NTD relative to the MD (Fig. 1). This movement rearranges (2200 Å^2) of surface buried between the NTD and MD. Although NTD displacement of HtpG by a model substrate protein has been linked to ATPase activation,[16] little is known about the molecular and

Additional Supporting Information may be found in the online version of this article.

*Correspondence to: Timothy O. Street, 415 South St., Brandeis University, Waltham, Massachusetts 02454. E-mail: tstreet@brandeis.edu

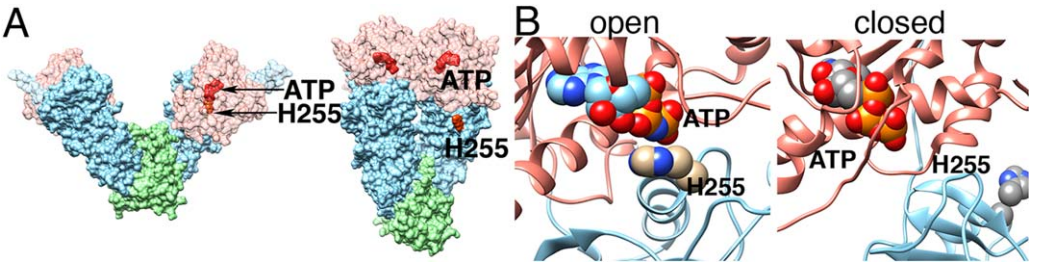

Figure 1. (A) H255 is in close contact with ATP in the open state (left: modeled from 1Y4S and 2IOQ), and is separated from ATP in the closed state (right: modeled from 2CG9). The NTD is semi-transparent. (B) A detailed view of the H255-ATP position.

energetic details that are responsible for NTD movement.

FRET measurements have shown that Hsp90 closure is slow relative to the subsequent ATP hydrolysis and reopening.[17] Indeed, non-hydrolysable nucleotide analogs such as AMPPNP and ATP-γS are required to shift Hsp90's population to a majority closed state.[17] Hsp90 nucleotide binding and dissociation rates are fast relative to closure,[18] making the binding K_d similar to the ATPase K_m. All Hsp90 homologs studied to date exhibit a slow ATPase on the order of 0.1–1/min.[2,19] This low rate implies a large energy barrier separating the open and closed states. Structural states of bacterial Hsp90 (HtpG), yeast Hsp90 (Hsp82) and human Hsp90 (Hsp90α) are conserved but the equilibria between these states are divergent.[20] Despite this underlying similarity among Hsp90 homologs, there is no current model of the dominant energetic factors that control Hsp90 conformational changes and ATPase rate. For example, although activating and inhibiting mutations have been identified,[6,7,21,22] a quantitative mechanistic explanation of why these mutations affect ATPase activity has been elusive.

While performing routine activity experiments, we discovered that HtpG displays a pH-dependent activity that is significantly different from other Hsp90 homologs. Here we show this behavior is due to a conserved molecular mechanism that regulates Hsp90 ATPase via a conformation-specific electrostatic interaction.

Results

pH-dependent activity of HtpG

Figure 2(A) shows dramatic pH-dependent activity of HtpG relative to other Hsp90 homologs such as Hsp82, Trap1 and Grp94. HtpG activity can be fully abrogated by a competitive inhibitor (not shown) indicating no contaminating ATPases. HtpG activity measured over a wide range of pH and ATP [Fig. 2(B)] shows that both k_{cat} and K_m are influenced by the pH [Fig. 2(C)].

Structural models of ATP-bound HtpG in the open and closed state immediately suggest the involvement of H255. In the open state, the nucleotide phosphate groups make close contact with H255, whereas H255 is 32 Å away from the nucleotide in the closed state (Fig. 1). A sequence alignment indicates that histidine at position 255 is unique to HtpG versus other Hsp90 homologs [Fig. 6(A)].

The H255A mutation exhibits an altered pH-dependence for both k_{cat} and K_m compared to wt HtpG (Fig. 3 inset, S1). Since H255A exhibits a residual pH-dependence we calculate the fold activation of H255A over the wild-type to determine the specific impact of H255. The resulting bell-shaped pH profile [Fig. 3(A)] suggests an underlying electrostatic mechanism whereby both the ATP phosphate group and H255 participate in a salt bridge interaction. Specifically, since both histidine and the ATP γ-phosphate are titratable, a salt bridge between these groups would only exist under the range of pH at which the histidine is positively charged and the ATP γ-phosphate is negatively charged.

The proposed salt-bridge explanation described above can be quantified in a linkage model, shown in Figure 3(B). The model includes the charge state of H255 (positive and neutral) and the ATP γ-phosphate (negative and neutral) with respective pK_a values. The salt bridge strength is quantified by an equilibrium constant, K_{sb}, or equivalently, energy $E_{sb} = -RT\ln(K_{sb})$. Since the H255-ATP salt bridge stabilizes the open configuration, E_{sb} is directly linked to pK_a shifts of both H255 and ATP in the open state, as demanded by thermodynamic cycles. More details of the model are discussed in Methods.

The solid line in Figure 3(A) shows a non-linear least squares fit of the linkage model [Eq. (2)] to the activity data. A sensitivity analysis demonstrates that the three adjustable parameters (pK_a^{His}, pK_a^{ATP}, E_{sb}) are uniquely determined from the data with no evidence of over fitting (Supporting Information Fig. S2). The fit parameters ($pK_a^{ATP} = 5.9$ and $pK_a^{His} = 7.1$) are comparable to literature values.[23,24] The salt bridge energy shifts the open state pK_a values in opposite directions ($pK_a^{ATP,\ open} = 4.9$, $pK_a^{His,\ open} = 8.1$), resulting in a broader range of pH over which the salt bridge can be formed. The salt bridge energy, $E_{sb} = -1.45$ kcal/mol, is in line with expectations for an electrostatic interaction. The salt bridge energy is

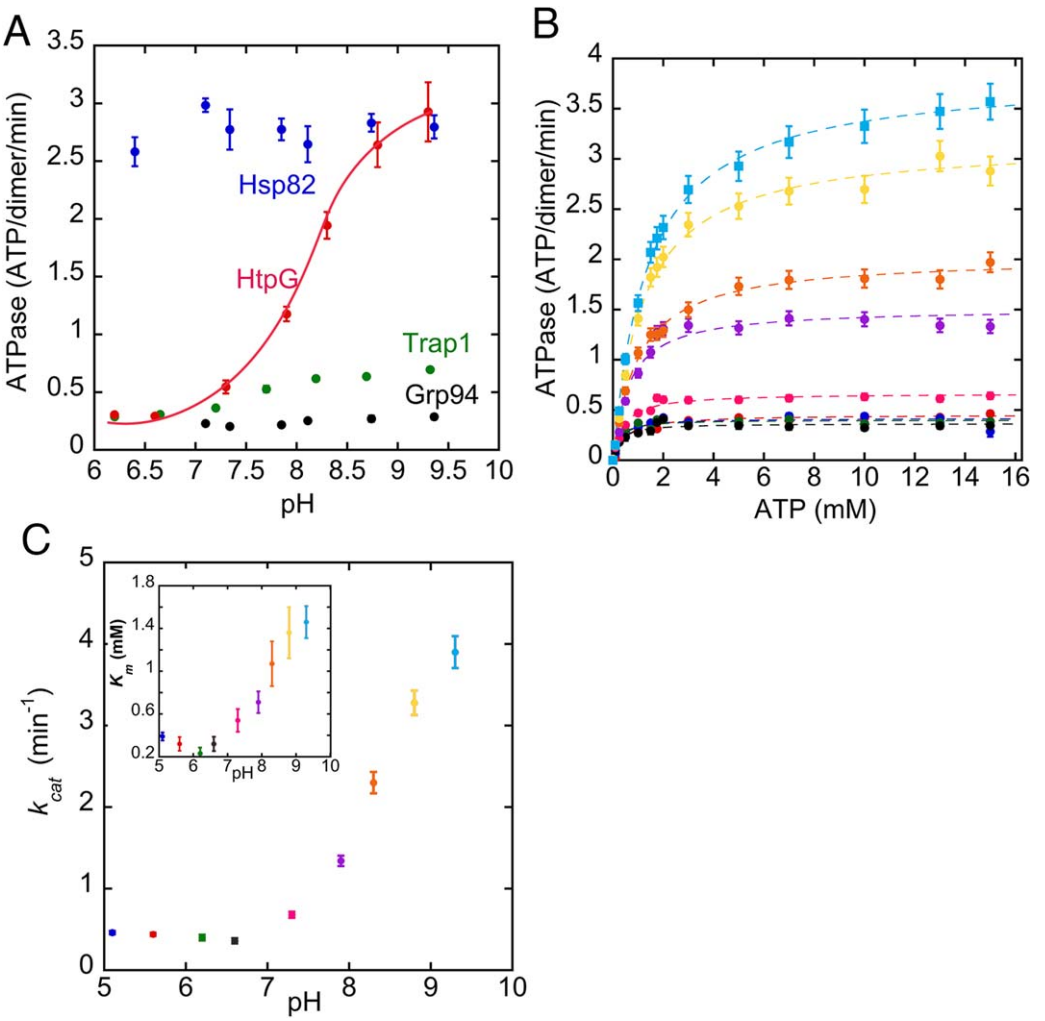

Figure 2. (A) HtpG activity (red circles) is pH-dependent, while Hsp82 and Grp94 are pH-independent and Trap1 has only a modest pH-dependence. Measurements were performed at a 1:1 stoichiometry of ATP:$MgCl_2$. The solid line is a visual guide. (B) HtpG Michaelis-Menten saturation curves at pH values between 5.1-9.3 (from low to high pH: blue, red, green, black, pink, purple, orange, yellow, and cyan). (C) The HtpG k_{cat} and K_m are both pH-dependent (colors are matched to panel B). Buffer conditions described in Methods. Error bars are the SEM for at least four measurements.

uniquely determined by the data, as illustrated by numerical simulations holding pK_a values fixed while varying E_{sb} [Fig. 3(C)].

Structural asymmetry in the HtpG activation mechanism

The fitting described above involves only one H255-ATP salt bridge, despite the dimer architecture of Hsp90. Although a model with two salt bridges could be constructed, we sought experimental evidence to determine the energetic contribution of one versus two salt bridges on the HtpG dimer.

To engineer one salt bridge per HtpG dimer, we constructed heterodimers with a mutant (D80N) known to prevent nucleotide binding.[6] Similar to established protocols,[22] HtpG heterodimers were constructed via a 9-fold excess of D80N followed by a long incubation to allow for monomer exchange (Methods). This experimental design enables the number of salt bridges to be directly compared against activity, as shown schematically in Figure 4(A). Here, the ATPase is reported by the active concentration of HtpG, that is, the ATPase is not normalized by the concentration of D80N.

At pH 6.6 [the pH of maximal ATPase enhancement by H255A, Fig. 3(A)] we find that the two salt-bridge dimer (wt homodimer) has similar activity as the one salt-bridge heterodimer (wt:D80N). In contrast, the one salt-bridge heterodimer (wt:D80N) is far less active than the zero salt bridge dimer (H255A homodimer), indicating that only one salt bridge per HtpG dimer is contributing to ATPase activation. The zero salt bridge dimer (H255A homodimer) has similar activity as the zero salt bridge heterodimer (H255A:D80N), demonstrating that the D80N construct does not interfere with activity on the opposite arm, consistent with previous observations.[25] As expected, D80N homodimer has no

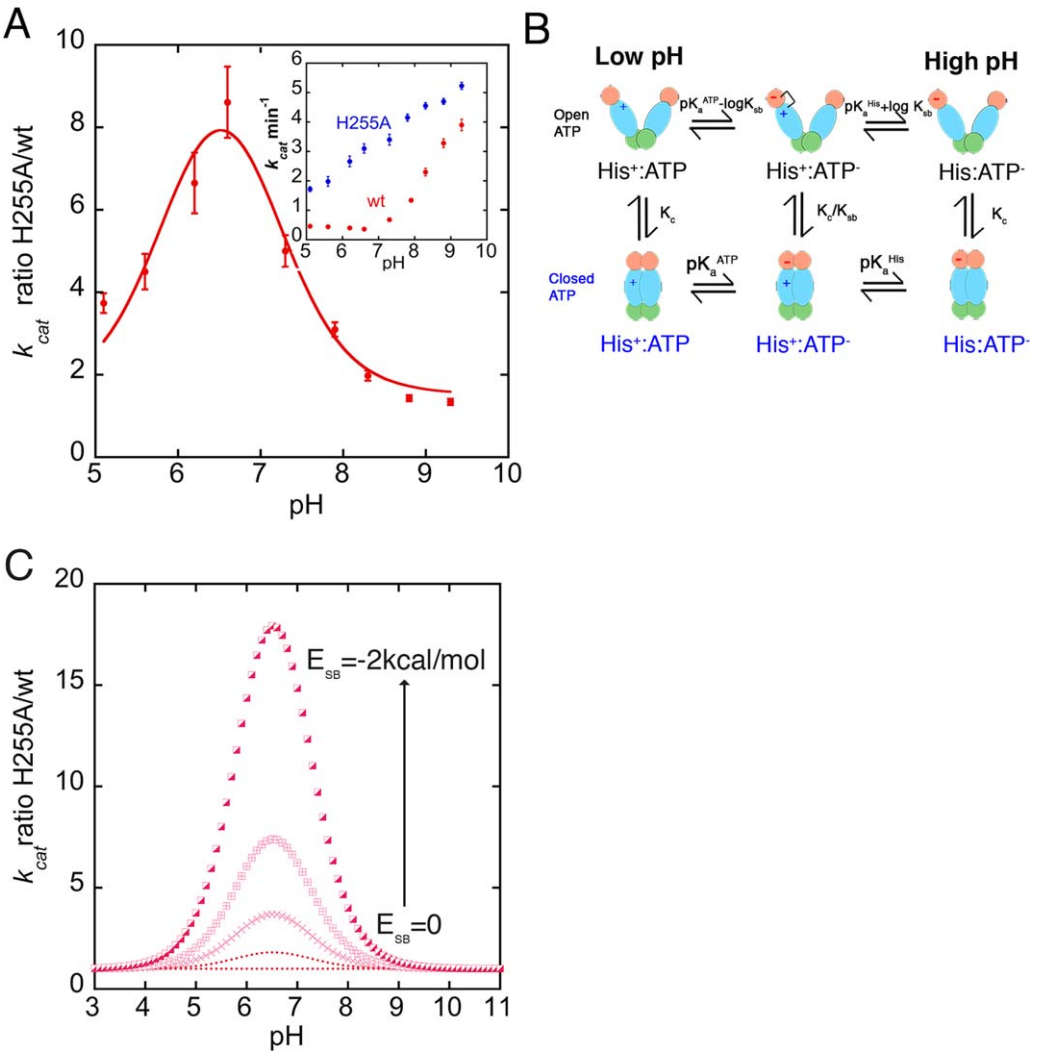

Figure 3. (A) The fold increase of H255A k_{cat} relative to HtpG has a bell-shaped pH profile. The solid line is a fit to Eq. (2). A comparison of k_{cat} values of HtpG and H255A are shown in the inset. Error bars are the SEM for at least four measurements. (B) Linkage model of HtpG pH-dependent activity. K_c represents the closure equilibrium constant. (C) Numerical simulations of the fold change of activity with fixed values of $pK_a^{His} = 5.9$ and $pK_a^{ATP} = 7.1$, and variable salt bridge energies of $E_{sb} = 0, -0.5, -1, -1.45, -2$ kcal/mol.

activity. As a further control, we measured the same constructs at pH 9.3, under which conditions all constructs have zero salt bridges, and as anticipated these constructs have comparable activity.

We conclude that the energetic contribution of the H255-ATP salt bridge is structurally asymmetric, whereby breaking only one H255-ATP salt-bridge per dimer of HtpG confers ATPase activation. More specifically, it is the transition between one salt-bridge and no salt-bridge that contributes to the closure energy barrier. We also conclude that the use of only a single salt bridge in the linkage model in Figure 3(B) is appropriate.

Anti-correlated nucleotide binding affinity and ATPase activity

The pH-dependent H255-ATP salt-bridge strongly represses activity by stabilizing ATP binding in the catalytically inactive open state. This mechanism suggests an energetic trade-off between ATP binding and ATPase activation. Indeed, numerical simulations (Methods) predict a simple reciprocal relationship between effective binding affinity (K_a) and k_{cat} (Supporting Information Fig. S3).

Our experimental data exhibits this predicted trade-off between affinity and activity. Specifically, we evaluated the impact of H255 on the effective K_a ($1/K_m$) from the Michaelis-Menten curves in Supporting Information Figure S1(A). The specific impact of H255 was calculated via the K_a ratio of H255A/wt. The resulting bell-shaped pH-profile [Fig. 5(A)] is similar in shape, but in the opposite direction, as the increase in k_{cat} in Figure 3(A). The reciprocal trade-off between affinity and activity is shown in Figure 5B. One outlier point is observed at the extreme low pH range (pH 5.1). The conclusion

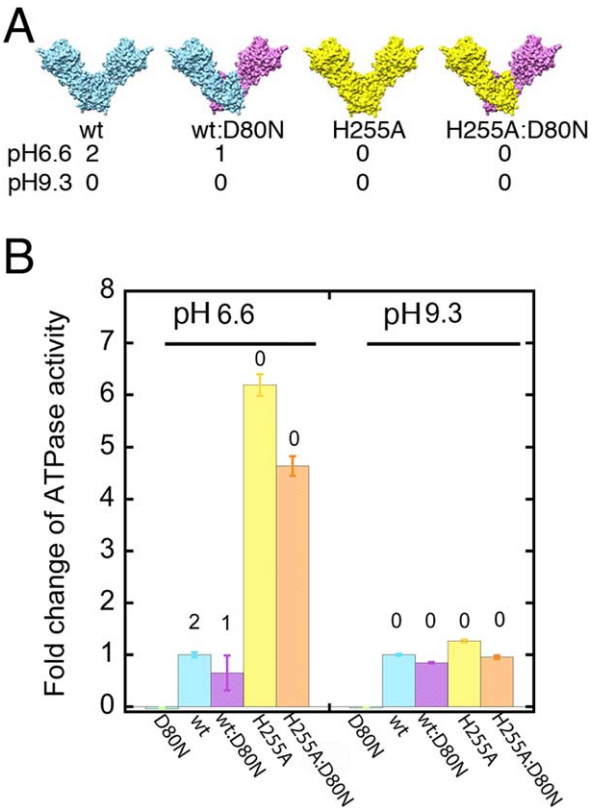

Figure 4. (A) HtpG heterodimer design. Homodimers and heterodimers of HtpG and H255A are shown with their respective number of H255-ATP salt bridges at high and neutral pH. (B) The relative activity of homodimers and heterodimers are normalized to the wt homodimer. The number of salt bridges for each construct is shown above the bar values. The ATP:$MgCl_2$ concentration is fixed at 5 mM. Propagated error calculated from the SEM for three measurements.

[shown qualitatively in Fig. 5(C)] is that H255 provides a mechanism by which nucleotide binding and the open-to-closed transition are in a direct energetic trade-off.

Evolutionarily conserved conformational energy landscape of Hsp90

The sequence alignment in Figure 6(A) illustrates that although a histidine at position 255 is only found in HtpG, a Grp94 lysine (K364) may form a similar salt bridge, albeit one that will not titrate over neutral pH. The K364 sidechain is not visible in the canine Grp94 open-state crystal structure, however, modeling shows that a K364-ATP interaction is possible [Fig. 6(B)]. The K364A mutant of Grp94 is activated four-fold, extending the underlying mechanism to the ER-resident family of Hsp90s.

The polar residue in the corresponding site of H255 in cytosolic Hsp90s (N298 for Hsp82) presents an opportunity to differentiate between an electrostatic interaction versus hydrogen bonding. The modest increase in activity for Hsp82 N298A [Fig. 6(C)] shows that hydrogen bonding provides a minimal stabilization of ATP in the open state. In contrast, N298H has strongly pH-dependent activity, similar to HtpG. This engineering of pH-dependent activity in Hsp82 extends the underlying conformational energy landscape to cytoplasmic Hsp90s.

Discussion

A working description of the ATP-driven conformational cycle of Hsp90 has emerged from the collective work of the multiple labs employing multiple experimental methods (crystallography, SAXS, FRET, EM, NMR).[11,17,20,26,27] The ATP-driven cycle is functionally important, as illustrated by Hsp82 mutations that are close to the ATP binding pocket having strong detrimental effects on yeast viability.[28] However, much less is known about the structural and energetic basis for the timing of Hsp90's progress through its conformational cycle. Revealing specific residues that control the Hsp90 conformational energy landscape is necessary for understanding regulation by co-chaperones, substrate proteins, and post-translational modifications.

Here, we discover that a single contact between H255 and ATP is responsible for pH-dependent HtpG activity. A linkage model describes how the titration of H255 and ATP results in a bell-shaped pH-dependent activity profile (Fig. 3). This model correctly predicts the observed anti-correlation between ATP binding affinity and activity (Supporting Information Fig. S3, 5). This is the first predictive model that connects Hsp90 structure to specific molecular contacts and their influence on the ATPase rate. Although H255 is unique to bacterial Hsp90, a similar underlying mechanism is present in Grp94 and can be engineered into Hsp82 (Fig. 6). We conclude that stabilizing interactions between the NTD and MD play a key role in controlling activity in the Hsp90 family.

The energetic contribution of the H255-ATP salt bridge is structurally asymmetric (Fig. 4). Specifically, it is the transition between one salt-bridge and no salt-bridges that contributes to the closure energy barrier. This observation suggests that compensating interactions can be formed after breaking the first salt-bridge. Our finding adds to a growing list of experimental measurements highlighting functional importance of asymmetry in Hsp90.[12,15,25]

SAXS measurements of HtpG previously identified a pH-dependent conformational change controlled by histidine 446.[29] Our finding of a second key histidine at the NTD/MD interface explains two previously mysterious observations from Krukenberg et al. (*i*) In the presence of AMPPNP the NTD + MD fragment alone exhibits a pH-dependent conformational change. (*ii*) In the presence of AMPPNP full-length HtpG exhibits a pH-dependent accumulation of the closed state, similar to our observed pH-

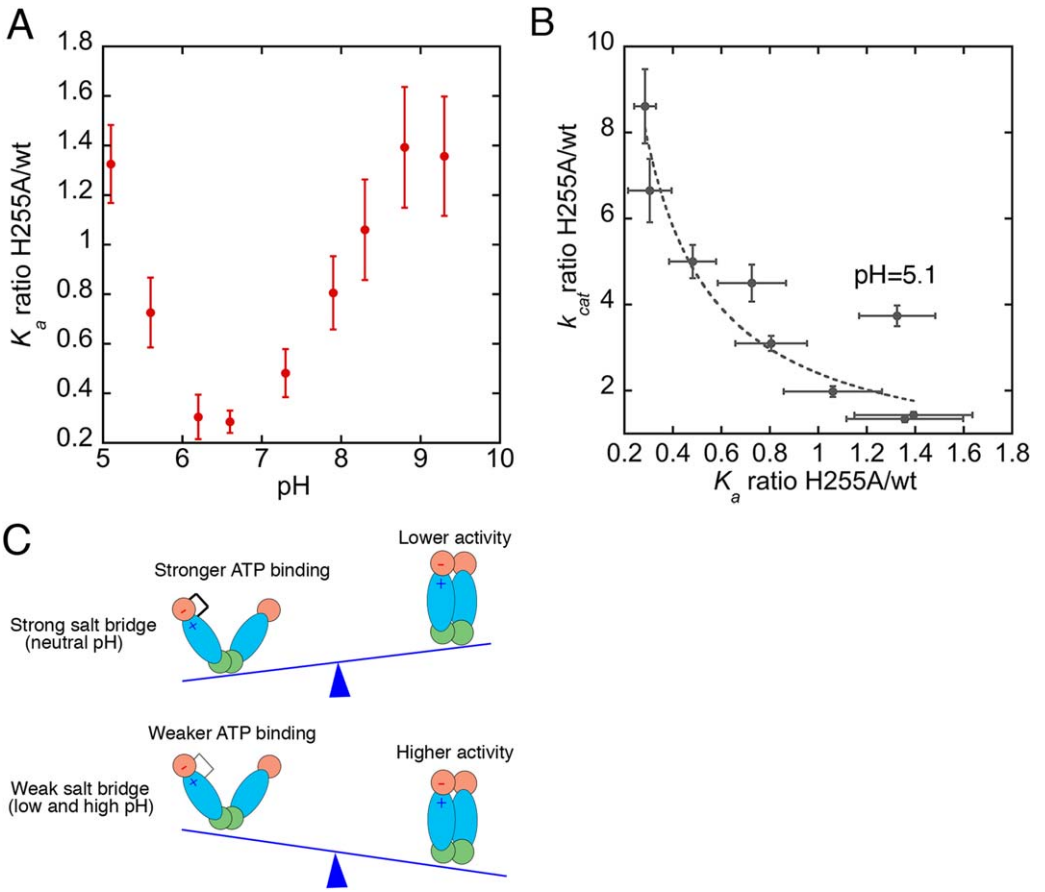

Figure 5. (A) Fold change of effective K_a ($1/K_m$) of H255A relative to HtpG. The bell-shaped pH profile is opposite in direction to the fold change of k_{cat} shown in Figure 3A. (B) The fold change of H255A k_{cat} relative to HtpG is inversely correlated with the fold change in effective K_a. The dashed line shows a fit to a reciprocal relationship. One outlier point is observed at pH 5.1. Error bars are the SEM for at least 4 measurements. (C) Schematic representation of H255 mechanism resulting in a trade-off between ATP binding and ATPase activation.

dependent activity (Fig. 2). More work is needed to determine the origin of the residual pH dependent activity of H255A.

H255 is not universally conserved in Hsp90 from bacteria. Rather, H255 is primarily found in Hsp90s from actinobacteria, proteobacteria, and spirochaetes, but is absent in cyanobacteria and firmicutes. The possible biological meaning behind this pattern of conservation is not yet clear. We speculate that the H255-ATP interaction mechanism allows HtpG to act as a "holdase" chaperone under acid shock conditions with a relatively low energy cost via keeping itself in an open inactive state.

Methods

HtpG and variants were expressed in *E. coli* BL21 cells. The vector, pET-151D, contains a 6 × His-tag and TEV cleavage site. Cells were grown at 37°C in LB and induced at OD_{600}=0.6∼0.8 with 1mM IPTG. HtpG and variants were purified by Ni-NTA affinity chromatography, followed by TEV cleavage of the His-tag, ion exchange chromatography (GE) and size-exclusion chromatography by superdex S-200 column (GE). SDS PAGE gels demonstrate complete digestion of the 6xHis-tag. Hsp82, Hsp90α, Grp94 were expressed and purified as previously described.[10,13,14] HtpG heterodimers were constructed via a 9-fold excess of D80N, followed by a 30 minute incubation at 30°C. The ATPase values in Figure 4(B) are normalized to the active concentration of HtpG or H255A monomer, similar to previously established methods.[25,30]

ATPase measurements

ATPase activity was measured with on a plate reader (BioTek) as previously described[12] with different buffers (pH 5.1–6.2 50 mM MES; pH 6.6 50 mM HEPES; pH 7.3–pH 9.3 50mM Tris). ATP hydrolysis rates of 1.5 μM dimer HtpG, Trap-1, Grp94, and Hsp82 were measured by the rate of NADH consumption via changes in absorption at 340nm. Activity measurements of HtpG, Trap-1, Grp94 and Hsp82 were performed at 25°C, 30°C, 40°C and 40°C, respectively. Assay components contained 400 μM NADH, 800 μM phosphoenolpyruvic (PEP), 50 U/ml

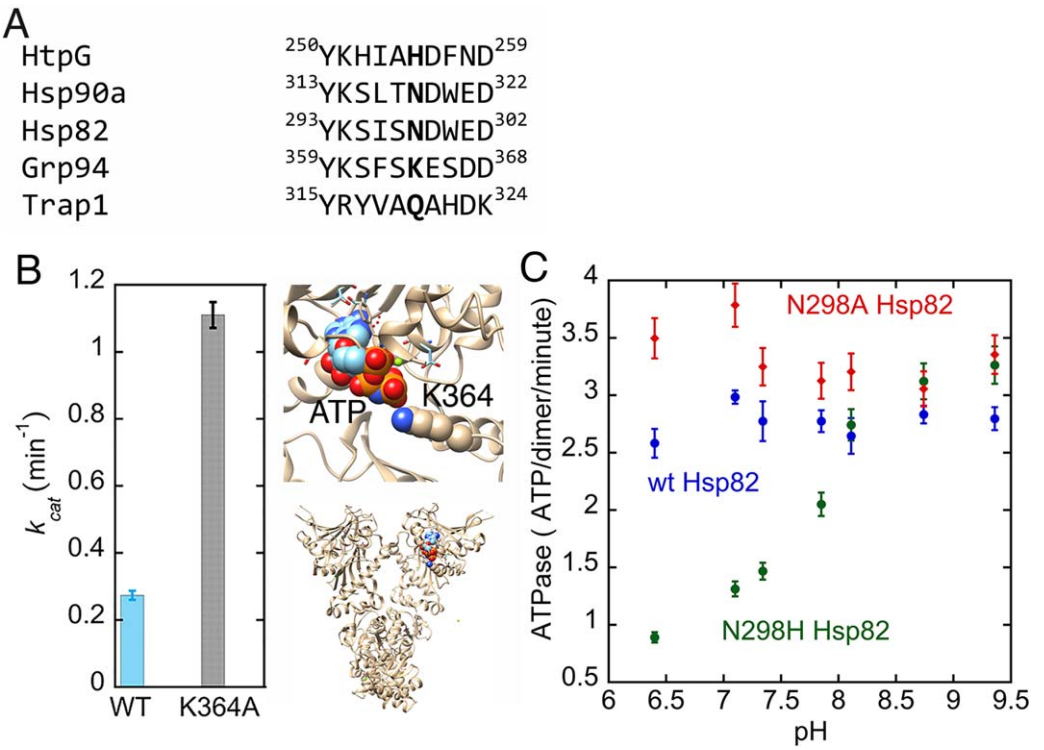

Figure 6. (A) Sequence alignment of Hsp90 homologs indicates that H255 is unique to HtpG. (B) The K364A variant of Grp94 activates the ATPase four-fold. A modelled position of K364, which is not visible in the 2IOU structure, shows it can reach ATP. C) The N298H variant of Hsp82 exhibits pH-dependent activity similar to HtpG. The N298A variant increases activity modestly. Error bars are the SEM for at least three measurements.

pyruvate kinase (PK), 50 U/ml lactate dehydrogenase (LDH) and 15 mg/mL BSA. 1 mM $CaCl_2$ was included in Grp94 activity measurements. For ATPase saturation measurements ATP and $MgCl_2$ were used in stoichiometric concentrations with 150 mM KCl. Activity data was fit by the Michaelis-Menten equation:

$$Activity = \frac{k_{cat} * [E]_0 * [ATP]}{K_m + [ATP]} \quad (1)$$

Linkage model curve fitting

The experimental data in Figure 3(A) is fit to a linkage model summarized in Figure 3(B). In addition to the six states that dominate the model, two additional states can be included for completeness (histidine neutral:ATP neutral, in both the open and closed states), although these states are not populated appreciably. Non-linear least squares curve fitting (Kaleidagraph) of the eight-state model was performed with the following equation:

$$A = \left(\frac{K_C}{1+K_C}\right)\frac{\left(10^{-pK_a^{His}+pH}+10^{-pK_a^{His}+pK_a^{ATP}}+10^{pK_a^{ATP}-pH}\right)\left(1+\frac{1}{K_c}\right)+1+K_{SB}/K_C}{10^{-pK_a^{His}+pH}+10^{-pK_a^{His}+pK_a^{ATP}}+10^{pK_a^{ATP}-pH}+1}+C \quad (2)$$

Where A is the fold increase of activity from removing the salt bridge in H255A. A derivation of Eq. (2) is shown in Supplemental Information. The fit parameters are pK_a^{His}, pK_a^{ATP}, K_{SB} and C. K_c is the open-to-closed equilibrium constant, which is set to a small value ($K_C \ll 1$) that favors the open state, as is observed experimentally.[17] Curve fitting results are independent of K_C if $K_C \ll 1$. An offset value, C, accounts for modest differences in activity of H255A and wild-type HtpG at high pH – this fit value is relatively small ($C = 0.51$).

Numerical simulations

Numerical simulations were performed in Matlab. The salt bridge energy calculations in Figure 3(C) utilized Eq. (2) with the experimentally-determined fit parameters ($pK_a^{ATP} = 5.9$ and $pK_a^{His} = 7.1$) and variable E_{sb} values over a wide range of pH.

To simulate the anti-correlation between K_a and k_{cat} (Supporting Information Fig. S3) we extended the linkage model to include apo open configurations. Michaelis Menten saturation curves were calculated under a wide range of pH using

experimentally determined values: $pK_a^{ATP} = 5.9$; $pK_a^{His} = 7.1$; $E_{sb} = -1.45$ kcal/mol. We set the high-pH K_a to 10^3, similar to the effective K_a ($1/K_m$) measured experimentally. Similar to other calculations, we set $K_C \ll 1$. Simulated saturation curves were fit to Eq. (1) to determine k_{cat} and K_m. Similar calculations were performed in the absence of a salt bridge ($E_{sb}=0$) to model H255A.

Acknowledgments

We thank members of the Street lab for helpful discussions. Research for this project was supported by R01 GM115356. The Authors have no conflict of interest to declare.

References

1. Young JC, Moarefi I, Hartl FU (2001) Hsp90: A specialized but essential protein-folding tool. J Cell Biol 154: 267–273.
2. Krukenberg KA, Street TO, Lavery LA, Agard DA (2011) Conformational dynamics of the molecular chaperone hsp90. Q Rev Biophys 44:229–255.
3. Taipale M, Krykbaeva I, Koeva M, Kayatekin C, Westover KD, Karras GI, Lindquist S (2012) Quantitative analysis of hsp90-client interactions reveals principles of substrate recognition. Cell 150:987–1001.
4. Richter K, Buchner J (2001) Hsp90: Chaperoning signal transduction. J Cell Physiol 188:281–290.
5. Pearl LH, Prodromou C (2006) Structure and mechanism of the hsp90 molecular chaperone machinery. Annu Rev Biochem 75:271–294.
6. Obermann WM, Sondermann H, Russo AA, Pavletich NP, Hartl FU (1998) In vivo function of hsp90 is dependent on ATP binding and ATP hydrolysis. J Cell Biol 143:901–910.
7. Panaretou B, Prodromou C, Roe SM, O'Brien R, Ladbury JE, Piper PW, Pearl LH (1998) Atp binding and hydrolysis are essential to the function of the hsp90 molecular chaperone in vivo. EMBO J 17:4829–4836.
8. Kamal A, Thao L, Sensintaffar J, Zhang L, Boehm MF, Fritz LC, Burrows FJ (2003) A high-affinity conformation of hsp90 confers tumour selectivity on hsp90 inhibitors. Nature 425:407–410.
9. Minami Y, Kimura Y, Kawasaki H, Suzuki K, Yahara I (1994) The carboxy-terminal region of mammalian hsp90 is required for its dimerization and function in vivo. Mol Cell Biol 14:1459–1464.
10. Richter K, Muschler P, Hainzl O, Buchner J (2001) Coordinated atp hydrolysis by the hsp90 dimer. J Biol Chem 276:33689–33696.
11. Ali MM, Roe SM, Vaughan CK, Meyer P, Panaretou B, Piper PW, Prodromou C, Pearl LH (2006) Crystal structure of an hsp90-nucleotide-p23/sba1 closed chaperone complex. Nature 440:1013–1017.
12. Lavery LA, Partridge JR, Ramelot TA, Elnatan D, Kennedy MA, Agard DA (2014) Structural asymmetry in the closed state of mitochondrial hsp90 (trap1) supports a two-step atp hydrolysis mechanism. Mol Cell 53:330–343.
13. Wolmarans A, Lee B, Spyracopoulos L, LaPointe P (2016) The mechanism of hsp90 atpase stimulation by aha1. Sci Rep 6:33179.
14. Retzlaff M, Hagn F, Mitschke L, Hessling M, Gugel F, Kessler H, Richter K, Buchner J (2010) Asymmetric activation of the hsp90 dimer by its cochaperone aha1. Mol Cell 37:344–354.
15. Mollapour M, Bourboulia D, Beebe K, Woodford MR, Polier S, Hoang A, Chelluri R, Li Y, Guo A, Lee MJ, et al. (2014) Asymmetric hsp90 n domain sumoylation recruits aha1 and atp-competitive inhibitors. Mol Cell 53:317–329.
16. Street TO, Lavery LA, Verba KA, Lee CT, Mayer MP, Agard DA (2012) Cross-monomer substrate contacts reposition the hsp90 n-terminal domain and prime the chaperone activity. J Mol Biol 415:3–15.
17. Hessling M, Richter K, Buchner J (2009) Dissection of the atp-induced conformational cycle of the molecular chaperone hsp90. Nat Struct Mol Biol 16:287–293.
18. McLaughlin SH, Ventouras LA, Lobbezoo B, Jackson SE (2004) Independent atpase activity of hsp90 subunits creates a flexible assembly platform. J Mol Biol 344:813–826.
19. Leskovar A, Wegele H, Werbeck ND, Buchner J, Reinstein J (2008) The atpase cycle of the mitochondrial hsp90 analog trap1. J Biol Chem 283:11677–11688.
20. Southworth DR, Agard DA (2008) Species-dependent ensembles of conserved conformational states define the hsp90 chaperone atpase cycle. Mol Cell 32:631–640.
21. Cunningham CN, Southworth DR, Krukenberg KA, Agard DA (2012) The conserved arginine 380 of hsp90 is not a catalytic residue, but stabilizes the closed conformation required for atp hydrolysis. Protein Sci 21: 1162–1171.
22. Cunningham CN, Krukenberg KA, Agard DA (2008) Intra- and intermonomer interactions are required to synergistically facilitate atp hydrolysis in hsp90. J Biol Chem 283:21170–21178.
23. Smith RM, Martell AE, Chen Y (1991) Critical-evaluation of stability-constants for nucleotide complexes with protons and metal-ions and the accompanying enthalpy changes. Pure Appl Chem 63: 1015–1080.
24. Thurlkill RL, Grimsley GR, Scholtz JM, Pace CN (2006) Pk values of the ionizable groups of proteins. Protein Sci 15:1214–1218.
25. Mishra P, Bolon DN (2014) Designed hsp90 heterodimers reveal an asymmetric atpase-driven mechanism in vivo. Mol Cell 53:344–350.
26. Krukenberg KA, Forster F, Rice LM, Sali A, Agard DA (2008) Multiple conformations of e-coli hsp90 in solution: Insights into the conformational dynamics of hsp90. Structure 16:755–765.
27. Zhang H, Zhou C, Chen W, Xu Y, Shi Y, Wen Y, Zhang N (2015) A dynamic view of ATP-coupled functioning cycle of hsp90 N-terminal domain. Sci Rep 5:9542.
28. Mishra P, Flynn JM, Starr TN, Bolon DN (2016) Systematic mutant analyses elucidate general and client-specific aspects of hsp90 function. Cell Rep 15:588–598.
29. Krukenberg KA, Southworth DR, Street TO, Agard DA (2009) pH-dependent conformational changes in bacterial hsp90 reveal a grp94-like conformation at ph 6 that is highly active in suppression of citrate synthase aggregation. J Mol Biol 390:278–291.
30. Richter K, Moser S, Hagn F, Friedrich R, Hainzl O, Heller M, Schlee S, Kessler H, Reinstein J, Buchner J (2006) Intrinsic inhibition of the hsp90 atpase activity. J Biol Chem 281:11301–11311.